Earthquake Spectra

DATA PAPER OPEN ACCESS

Experimental Dataset From Full-Scale Near-Collapse Tests on Two-Storey, Two-Bay Masonry-Infilled Reinforced Concrete Frames With Timber-Based Reinforced Concrete-Timber Panel Seismic Retrofit

Nikolaos Stathas[1] | Andrea Bartolotti[2] | Nicolò Damiani[3,4] | Stathis Bousias[1] | Francesco Smiroldo[2] | Albino Angeli[5] | Dmytro Dizhur[6] | Francesco Graziotti[3,4] | Ivan Giongo[2]

[1]Department of Civil Engineering, University of Patras, Patras, Greece | [2]Department of Civil, Environmental and Mechanical Engineering, University of Trento, Trento, Italy | [3]Department of Civil Engineering and Architecture, University of Pavia, Pavia, Italy | [4]European Centre for Training and Research in Earthquake Engineering (EUCENTRE), Pavia, Italy | [5]XLAM DOLOMITI S.p.a., Trento, Italy | [6]PYTHON Fixings Ltd, Auckland, New Zealand

Correspondence: Nikolaos Stathas (stathas@upatras.gr)

Received: 10 November 2025 | **Revised:** 3 March 2026 | **Accepted:** 26 March 2026

Keywords: cross-laminated timber | existing reinforced concrete frames | full-scale quasi-static cyclic testing | masonry infills | timber-based seismic retrofit

ABSTRACT

This study describes a dataset from an experimental campaign investigating the quasi-static cyclic lateral response of two full-scale, two-storey, two-bay reinforced concrete (RC) frames with masonry infills representative of mid-20th century European construction practice. The nominally identical specimens were tested in both as-built and retrofitted configurations. The dataset aims to provide new experimental evidence on the investigation of the effectiveness of a cross-laminated timber (CLT)-based retrofit system, in which the external masonry wythe is replaced by a CLT panel connected to the RC frame through a glulam subframe and dissipative fasteners, while the internal wythe is retained to ensure compatibility with finishing layers. The campaign comprises snap-back tests to characterize initial dynamic properties and quasi-static cyclic tests conducted up to near-collapse conditions. The dataset includes actuator forces and displacements, local deformations of masonry infills and CLT panels, relative slip at connections and material characterization tests. The work presented aims at contributing to the calibration and validation of numerical/analytical models and, possibly, to the development of guidelines for integrated seismic and energy renovation of existing infilled RC framed buildings.

1 | Introduction

Mid-20th century-reinforced concrete (RC) frame buildings with masonry infills represent a large portion of the European building stock and are known to exhibit significant seismic vulnerabilities (Sezen et al. 2003; Ricci et al. 2011; Masi et al. 2019; Demirel et al. 2022; Vuran et al. 2025). In many cases these structures were designed without seismic provisions and are characterized by poor detailing, such as insufficient transverse reinforcement and nonductile beam–column joints, leading to brittle local failures and limited global ductility (Pampanin et al. 2002; Hassan and Moehle 2012; Pavese et al. 2016).

In recent years, timber-based retrofit solutions have gained increasing attention due to their structural efficiency, sustainability, and potential for prefabrication and rapid installation (Meireis et al. 2022; Iovane et al. 2023; Giongo, Graziotti, Marini et al. 2025).

Previous research has already provided valuable insights through advanced numerical simulations (Smiroldo et al. 2021; Bartolotti et al. 2024) and experimental campaigns on single-storey, single-bay RC frames retrofitted with timber panels (a technique referred to as RC-TP) tested up to a near-collapse condition (Smiroldo et al. 2023). These studies have demonstrated the potential of the RC–TP technique, where masonry infills are either replaced or partially replaced by cross-laminated timber (CLT) panels connected to the RC frame through a glulam subframe and dissipative fasteners, to improve the seismic performance of existing buildings. Additionally, experimental tests on multi-storey, multi-bay frames were performed using the pseudodynamic (PsD) testing method with substructuring (Kallioras et al. 2024). However, evidence at the scale of multi-storey, multi-bay frames subjected to incipient collapse conditions in the pre- and post-intervention configuration has so far been missing.

The STRONG (*Sustainable TimbeR retrOfit of concrete buildinGs*) project, carried out within the ERIES (*Engineering Research Infrastructures for European Synergies*) Transnational Access program, was specifically conceived to fill this gap. The RC–TP retrofit has been applied and tested up to specimen failure on a two-storey, two-bay RC frame designed to replicate mid-20th century construction practices. Compared with earlier campaigns, the present program introduces the following novel aspects:

- The retention of the internal (weak) wythe of the masonry infill in a test conducted until specimen near-collapse conditions.
- The presence of various joint types (e.g., external and knee beam-column joints), whose response was monitored up to the attainment of specimen ultimate conditions.
- The use of dry mechanical screw connections between the RC frame and the glulam subframe.
- The compatibility of the intervention with finishing nonstructural layers such as ventilated façade systems.

FIGURE 1 | Experimental campaign: full-scale two-storey, two-bay RC frames.

The main objective of the campaign was to investigate the seismic performance of a retrofitted specimen against that of an as-built reference frame under identical boundary conditions and progressively increasing in-plane cyclic loading. Equally important, the program was designed with a strong data-oriented purpose. The comprehensive dataset generated from these tests is described in detail regarding the measured parameters, the type and the location of the sensors used to capture completely and effectively the response of the two specimens. Subsequently, the dataset will potentially contribute not only to the calibration and validation of numerical and analytical models, but also to the development of guidelines for integrated seismic and energy renovation of existing infilled RC framed structures.

The novelty of the STRONG dataset lies not only in the type and experimental scale of the specimens, but also in its intention: to provide transparent and reusable data on an innovative timber-based retrofit technique with direct applicability to widespread vulnerable building typologies across Europe.

2 | The Experimental Campaign

The experimental campaign was conceived to investigate the seismic response of full-scale, two-storey, two-bay RC frames, both in their as-built (Figure 1a) and retrofitted (Figure 1b) configurations, under a quasi-static cyclic loading protocol up to failure.

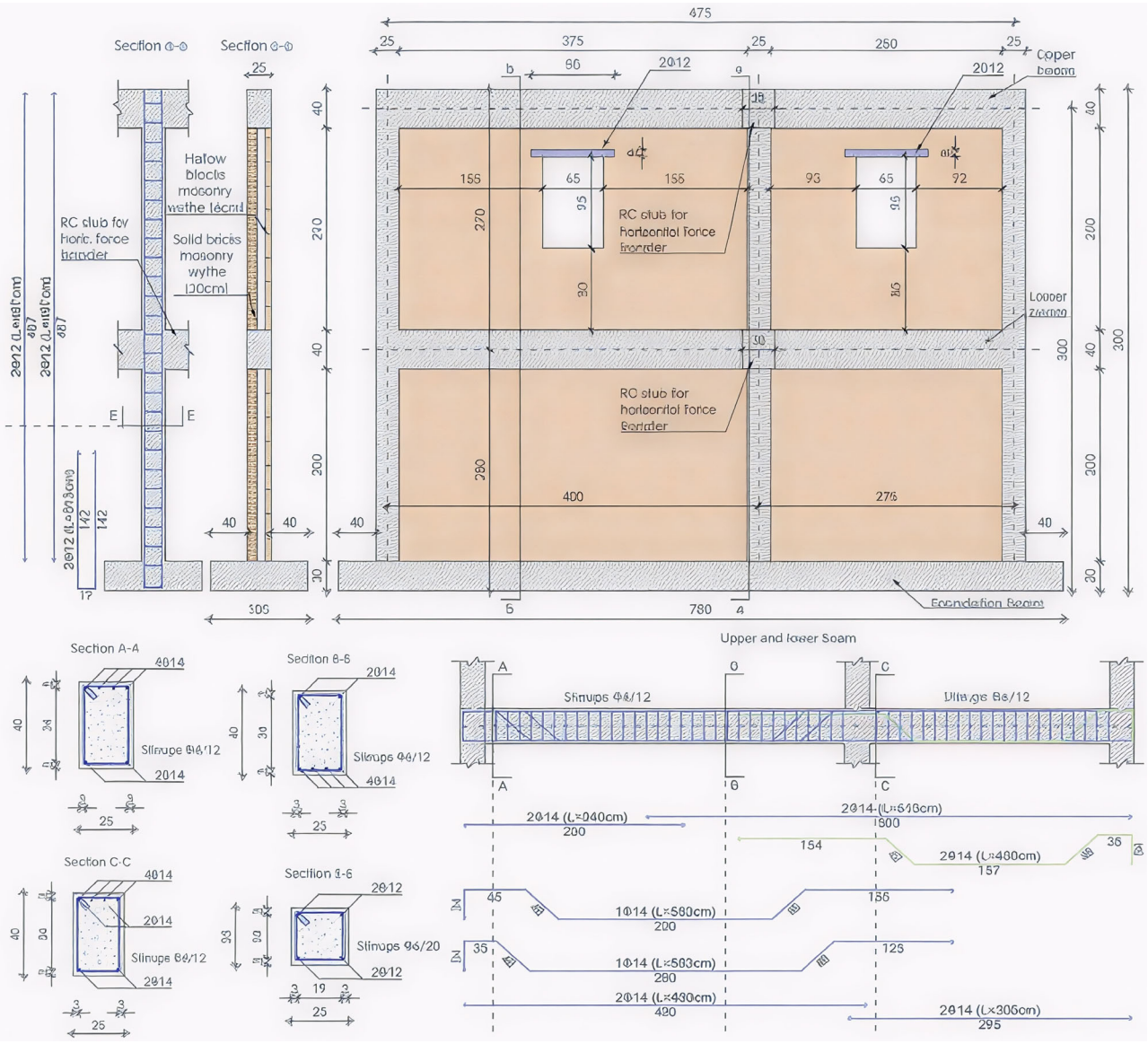

FIGURE 2 | Geometry and reinforcement layout of as-built and retrofitted specimen.

TABLE 1 | Material properties data.

Property	Mean value	C.o.V., %
Compressive strength of concrete cubes	15.6 MPa	7.4
Tensile strength of longitudinal reinforcing bars	278.7 MPa	7.6
Tensile strength of transverse reinforcing bars	323.1 MPa	0.6
Flexural strength of mortar prisms	1.8 MPa	23.5
Compressive strength of mortar prisms	3.8 MPa	33.9
Compressive strength of solid clay bricks	24.8 MPa	17.3
Compressive strength of hollow clay blocks	8.5 MPa	26.6
Compressive strength of solid clay bricks masonry prisms	7.4 MPa	19.3
Compressive strength of hollow clay blocks masonry prisms	1.4 MPa	10.9
Shear strength of solid clay bricks masonry triplets with constant compression equal to 0.2 MPa	0.6 MPa	22.2
Shear strength of hollow clay blocks masonry triplets with constant compression equal to 0.1 MPa	0.4 MPa	34
Pull-out strength of timber-to-concrete connections	51.4 kN	4.2
Push-out strength of timber-to-concrete connections	18.4 kN	8.2

TABLE 2 | Nominal mechanical characteristics of CLT panel of thickness equal to 57 mm (three orthotropic layers of equal thickness).

Direction	Bending strength	Tensile strength	Compressive strength	Shear strength
Perpendicular to CLT[a]	26.4 MPa, parallel to the grain of the boards	0.12 MPa, perpendicular to the grain of the boards	2.5 MPa, perpendicular to the grain of the boards	4.0 MPa, parallel to the grain of the boards 1.8 MPa, perpendicular to the grain of the boards
In plane of CLT[a]	24.0 MPa, parallel to the grain of the boards	14.0 MPa, parallel to the grain of the boards	21.0 MPa, parallel to the grain of the boards	3.3 MPa, parallel to the grain of the boards

[a]The above values were provided by X-LAM DOLOMITI, European Technical Assessment (ETA-12/0347).

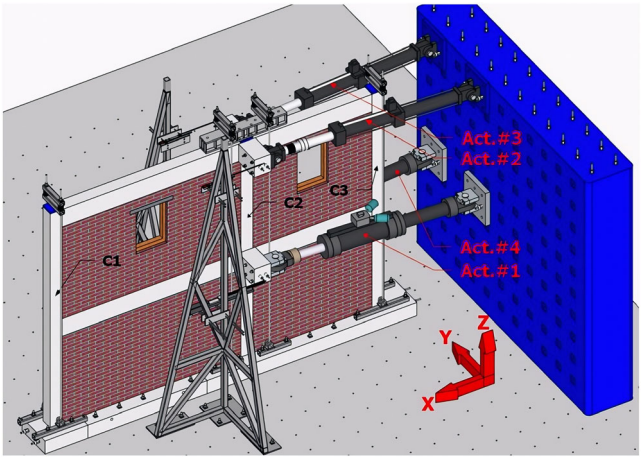

FIGURE 3 | Cyclic test setup.

A preliminary stage consisted of snap-back tests, performed before the onset of damage, with the aim of estimating the initial stiffness, natural frequencies, and damping properties of the frames.

Subsequently, the as-built specimen was subjected to two distinct cyclic tests (Stage 1 and Stage 2). In Stage 1, the lateral forces were applied according to the inverted triangular distribution described in Section 2.2, and loading was continued until the upper storey reached ultimate conditions. In Stage 2, the control strategy was modified so that the first storey was actively loaded while the upper one was only deformed by the displacement imposed at the lower level, until failure occurred at the first storey. This two-step approach enabled a clearer interpretation of the respective contribution of the two storeys to the overall collapse mechanisms.

For the retrofitted specimen, two consecutive cyclic tests were performed on the same frame in order to evaluate the influence of connection details on the efficiency of the RC-TP system. In Stage 1, the CLT panel-to-subframe connection was realized with screws installed without washers, representing a common yet less efficient fastening configuration. After this test, which already induced a certain level of damage in the specimen, the connection system was improved by adding washers to all screws and introducing an additional number of fasteners between the CLT panel and the glulam subframe. Stage 2, carried out on the same specimen, allowed the direct quantification of the beneficial effect of these modifications in terms of stiffness, strength, ductility, and relative slip control.

This testing program, articulated in successive stages on both the as-built and the retrofitted specimens, was designed to provide complementary insights into the seismic response, damage progression, and ultimate failure modes of the investigated structural typologies.

2.1 | Tested Specimens

The two specimens tested in the campaign were designed as two-storey, two-bay RC frames with geometrical and material properties representative of Mediterranean construction practice of the 1950s–1970s. The as-built configuration was completed with cavity masonry infills, composed of an external wythe of solid clay bricks and an internal wythe of hollow clay blocks, while the retrofitted specimen followed the RC–TP scheme, in which the external wythe was removed and replaced by a CLT panel connected through a glulam subframe and dissipative fasteners.

A distinctive feature of this program, compared with previous experiments where frames reached incipient collapse conditions (Smiroldo et al. 2023), was the inclusion of window openings, the use of dry mechanical connections between RC frame and timber subframe, and the retention of the internal masonry wythe, which was mechanically tied to the CLT panels to prevent out-of-plane instability. Dimension-wise, both the as-built and retrofitted specimens were identical—the

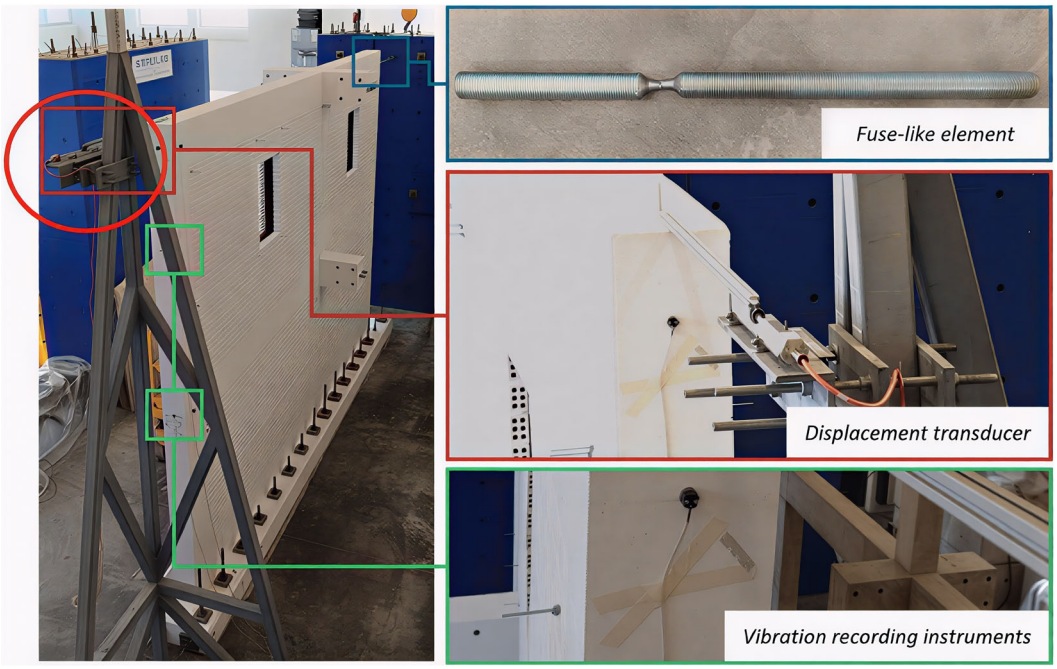

FIGURE 4 | Snap-back tests setup.

same holds for the reinforcement of the RC frames. The geometry and reinforcement layout are presented in Figure 2. A comprehensive testing campaign to characterize the mechanical properties of materials and connections was also performed comprising compression tests on concrete cubes, tensile tests on reinforcing bars, flexural and compression tests on mortar prisms, compression tests on bricks and blocks, compression tests on masonry prisms, shear tests on masonry triplets, and pull-out and cyclic/monotonic pushout tests on timber-to-concrete connections (Tables 1 and 2). For further information the reader is referred to Giongo, Graziotti, Stathas, et al. (2025).

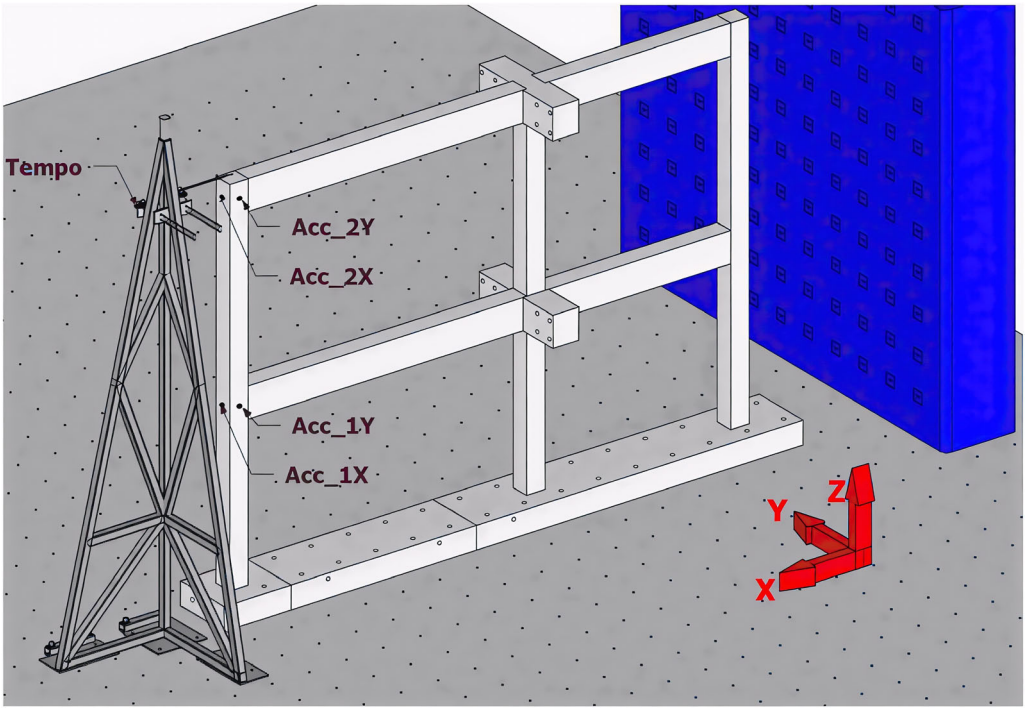

FIGURE 5 | Snap-back test setup illustrating the instrumentation layout, including accelerometers and the high-accuracy displacement transducer (Tempo).

TABLE 3 | Test names, data file names, and data matrix dimensions.

Test no.	Test name	Data file name (*.csv)	Data matrix size
1	AsBuilt specimen Snapback test	ERIES_STRONG_AsBuilt_Snapback	$44{,}349 \times 5$, $89{,}820 \times 2$
2	AsBuilt specimen Stage1	ERIES_STRONG_AsBuilt_Stage1	4362×47
3	AsBuilt specimen Stage2	ERIES_STRONG_AsBuilt_Stage2	4614×13
4	Retrofitted specimen Snapback test	ERIES_STRONG_ Retrofitted _Snapback	$43{,}692 \times 5$, $82{,}345 \times 2$
5	Retrofitted specimen Stage1	ERIES_STRONG_ Retrofitted_Stage1	1342×112
6	Retrofitted specimen Stage2	ERIES_STRONG_ Retrofitted_Stage2	1960×112

TABLE 4 | Metadata for sensors in the "AsBuilt_Snapback" and "Retrofitted_Snapback" files.

Col.	Instrument ID	Description	Remarks
1	Tempo	Displacement [mm]	—
2	Acc_1X	First-story acceleration, X direction [g]	—
3	Acc_2X	Second-story acceleration, X direction	—
4	Acc_1Y	First-story acceleration, Y direction	—
5	Acc_2Y	Second-story acceleration, Y direction	—

TABLE 5 | Metadata for sensors in the "AsBuilt_Stage1" and "AsBuilt_Stage2" files.

Col.	Instrument ID	Description	Remarks
2	Act. #1	Actuator force [kN]	—
3	Act. #2	Actuator force [kN]	—
4	Act. #3	Actuator force [kN]	—
5	Act. #4	Actuator force [kN]	—
6	Act. #1	Actuator displacement [mm]	—
7	Act. #2	Actuator displacement [mm]	—
8	Act. #3	Actuator displacement [mm]	—
9	Act. #4	Actuator displacement [mm]	—
10	POT 13	External infill deformation, 2nd storey [mm]	—
11	POT 14	External infill deformation, 2nd storey [mm]	—
12	POT 15	External infill deformation, 2nd storey [mm]	—
13	POT 16	External infill deformation, 2nd storey [mm]	—
14	POT 17	External infill deformation, 2nd storey [mm]	—
15	POT 18	External infill deformation, 2nd storey [mm]	—
16	POT 19	External infill deformation, 2nd storey [mm]	[a]
17	POT 22	External infill deformation, 2nd storey [mm]	—
18	POT 23	External infill deformation, 2nd storey [mm]	—
19	POT 24	External infill deformation, 2nd storey [mm]	—
20	POT 28	External infill deformation, 2nd storey [mm]	—
21	POT 29	External infill deformation, 2nd storey [mm]	—
22	POT 32	External infill deformation, 2nd storey [mm]	—
23	POT 33	External infill deformation, first storey [mm]	—
24	POT 36	Internal infill deformation, 2nd storey [mm]	—
25	POT 37	External infill deformation, 2nd storey [mm]	—
26	POT 39	Internal infill deformation, first storey [mm]	—
27	POT 40	Internal infill deformation, 2nd storey [mm]	—
28	POT 41	External infill deformation, 2nd storey [mm]	—
29	POT 43	External infill deformation, 2nd storey [mm]	—
30	POT 44	External infill deformation, 1st storey [mm]	—
31	POT 45	External infill deformation, 2nd storey [mm]	—
32	POT 52	Internal infill deformation, 1st storey [mm]	—
33	POT 75	External infill deformation, 2nd storey [mm]	—
34	SPR-POT 1	Foundation uplift [mm]	—
35	SPR-POT 3	Frame out-of-plane displacement [mm]	n/a
36	SPR-POT 4	Foundation slip [mm]	—
37	SPOT 1	External infill deformation, 1st storey [mm]	—
38	SPOT 2	External infill deformation, 1st storey [mm]	—
39	SPOT 4	Internal infill deformation, 2nd storey [mm]	[a]
40	SPOT 9	External infill deformation, 2nd storey [mm]	—
41	SPOT 12	Internal infill deformation, 1st storey [mm]	—
42	SPOT 13	External infill deformation, 2nd storey [mm]	—
43	SPOT 14	Internal infill deformation, 1st storey [mm]	—

(Continues)

TABLE 5 | (Continued)

Col.	Instrument ID	Description	Remarks
44	SPOT 15	Internal infill deformation, 2nd storey [mm]	—
45	C1	Column C1 axial force [kN]	n/a
46	C2	Column C2 axial force [kN]	n/a
47	C3	Column C3 axial force [kN]	n/a

[a]Instrument readings exhibit drift, likely related to tip friction or movement.

TABLE 6 | Metadata for sensors in the "Retrofitted_Stage1" and "Retrofitted_Stage2" files.

Col.	Instrument ID	Description	Remarks
1	Act. #1	Actuator force [kN]	—
2	Act. #2	Actuator force [kN]	—
3	Act. #3	Actuator force [kN]	—
4	Act. #4	Actuator force [kN]	—
5	Act. #1	Actuator displacement [mm]	—
6	Act. #2	Actuator displacement [mm]	—
7	Act. #3	Actuator displacement [mm]	—
8	Act. #4	Actuator displacement [mm]	—
9	POT 1	RC-CLT relative vertical displacement, 2nd storey [mm]	—
10	POT 2	RC-CLT relative vertical displacement, 2nd storey [mm]	[a]
11	POT 3	RC-CLT relative horizontal displacement, 1st storey [mm]	—
12	POT 4	RC-CLT relative horizontal displacement, 2nd storey [mm]	—
13	POT 5	RC-CLT relative horizontal displacement, 1st storey [mm]	[b]
14	POT 6	RC-CLT relative horizontal displacement, 2nd storey [mm]	—
15	POT 7	RC-CLT relative horizontal displacement, 1st storey [mm]	[b]
16	POT 8	RC-CLT relative horizontal displacement, 2nd storey [mm]	[a]
17	POT 10	RC-CLT relative vertical displacement, 1st storey [mm]	—
18	POT 11	RC-CLT relative vertical displacement, 2nd storey [mm]	—
19	POT 12	RC-CLT relative vertical displacement, 1st storey [mm]	[a]
20	POT 13	CLT deformation, 2nd storey [mm]	—
21	POT 14	CLT deformation, 2nd storey [mm]	n/a
22	POT 15	CLT deformation, 2nd storey [mm]	[a]
23	POT 16	CLT deformation, 2nd storey [mm]	–
24	POT 17	CLT deformation, 2nd storey [mm]	n/a
25	POT 18	CLT deformation, 2nd storey [mm]	—
26	POT 19	CLT deformation, 2nd storey [mm]	—
27	POT 20	RC-CLT relative vertical displacement, 2nd storey [mm]	—
28	POT 21	RC-GLT relative vertical displacement, 2nd storey [mm]	—
29	POT 22	CLT deformation, 2nd storey [mm]	—
30	POT 23	CLT deformation, 2nd storey [mm]	—
31	POT 25	RC-GLT relative vertical displacement, 2nd storey [mm]	—
32	POT 26	RC-GLT relative vertical displacement, 2nd storey [mm]	—

(Continues)

TABLE 6 | (Continued)

Col.	Instrument ID	Description	Remarks
33	POT 27	RC-GLT relative horizontal displacement, 1st storey [mm]	—
34	POT 28	CLT deformation, 2nd storey [mm]	—
35	POT 29	CLT deformation, 2nd storey [mm]	n/a
36	POT 30	RC-CLT relative vertical displacement, 1st storey [mm]	—
37	POT 31	RC-CLT relative horizontal displacement, 1st storey [mm]	b
38	POT 32	CLT deformation, 2nd storey [mm]	—
39	POT 33	CLT deformation, 1st storey [mm]	—
40	POT 34	RC-CLT relative horizontal displacement, 1st storey [mm]	—
41	POT 35	RC-CLT relative vertical displacement, 2nd storey [mm]	—
42	POT 36	Internal infill deformation, second storey [mm]	—
43	POT 37	Frame out-of-plane displacement [mm]	—
44	POT 38	RC-CLT relative horizontal displacement, second storey [mm]	c
45	POT 39	Internal infill deformation, 1st storey [mm]	d
46	POT 40	Internal infill deformation, 2nd storey [mm]	—
47	POT 41	CLT deformation, 2nd storey [mm]	—
48	POT 43	CLT deformation, 2nd storey [mm]	—
49	POT 44	CLT deformation, 1st storey [mm]	—
50	POT 45	CLT deformation, 2nd storey [mm]	—
51	POT 46	RC-GLT relative horizontal displacement, 1st storey [mm]	—
52	POT 47	RC-CLT relative vertical displacement, 1st storey [mm]	—
53	POT 48	RC-CLT relative horizontal displacement, 1st storey [mm]	b
54	POT 49	RC-CLT relative horizontal displacement, 2nd storey [mm]	—
55	POT 50	RC-CLT relative vertical displacement, 1st storey [mm]	—
56	POT 51	RC-GLT relative vertical displacement, 1st storey [mm]	—
57	POT 52	Internal infill deformation, 1st storey [mm]	e
58	POT 53	RC-CLT relative horizontal displacement, 2nd storey [mm]	—
59	POT 54	RC-GLT relative vertical displacement, 2nd storey [mm]	—
60	POT 55	RC-CLT relative horizontal displacement, 1st storey [mm]	—
61	POT 56	RC-CLT relative horizontal displacement, 1st storey [mm]	b,e
62	POT 57	RC-CLT relative horizontal displacement, 2nd storey [mm]	—
63	POT 58	RC-CLT relative vertical displacement, 1st storey [mm]	—
64	POT 59	RC-GLT relative horizontal displacement, 1st storey [mm]	—
65	POT 60	RC-CLT relative vertical displacement, 2nd storey [mm]	—
66	POT 61	RC-CLT relative vertical displacement, 2nd storey [mm]	—
67	POT 62	RC-GLT relative vertical displacement, 1st storey [mm]	—
68	POT 63	RC-GLT relative vertical displacement, 2nd storey [mm]	—
69	POT 64	RC-GLT relative vertical displacement, 2nd storey [mm]	—
70	POT 65	RC-GLT relative horizontal displacement, 1st storey [mm]	c,d
71	POT 66	RC-GLT relative vertical displacement, 1st storey [mm]	—
72	POT 67	RC-GLT relative vertical displacement, 1st storey [mm]	d
73	POT 68	RC-GLT relative horizontal displacement, 1st storey [mm]	—

(Continues)

TABLE 6 | (Continued)

Col.	Instrument ID	Description	Remarks
74	POT 69	RC-GLT relative vertical displacement, 1st storey [mm]	[d]
75	POT 70	RC-GLT relative horizontal displacement, 1st storey [mm]	—
76	POT 71	RC-GLT relative vertical displacement, 2nd storey [mm]	[d]
77	POT 72	RC-GLT relative vertical displacement, 1st storey [mm]	—
78	POT 73	RC-GLT relative vertical displacement, 2nd storey [mm]	—
79	POT 74	RC-GLT relative horizontal displacement, 1st storey [mm]	—
80	POT 75	CLT deformation, second storey [mm]	—
81	POT 76	RC-GLT relative vertical displacement, 1st storey [mm]	[d]
82	POT 77	RC-CLT relative vertical displacement, 2nd storey [mm]	—
83	POT 111	RC-GLT relative vertical displacement, 1st storey [mm]	[d]
84	POT 222	RC-CLT relative horizontal displacement, 2nd storey [mm]	—
85	SPR-POT 1	Foundation uplift [mm]	—
86	SPR-POT 2	RC-GLT relative horizontal displacement, 1st storey [mm]	—
87	SPR-POT 3	Foundation slippage [mm]	—
88	SPR-POT 4	RC-CLT relative vertical displacement, 1st storey [mm]	[d]
89	SPR-POT 5	RC-CLT relative vertical displacement, 1st storey [mm]	—
90	SPR-POT 6	RC-GLT relative horizontal displacement, 2nd storey [mm]	[c]
91	SPR-POT 7	RC-GLT relative horizontal displacement, 2nd storey [mm]	[c]
92	SPR-POT 9	RC-GLT relative horizontal displacement, 2nd storey [mm]	—
93	SPR-POT 10	RC-GLT relative horizontal displacement, 2nd storey [mm]	—
94	SPR-POT 11	RC-GLT relative horizontal displacement, 2nd storey [mm]	—
95	SPR-POT 12	RC-GLT relative horizontal displacement, 2nd storey [mm]	[c]
96	SPR-POT 14	RC-GLT relative horizontal displacement, 2nd storey [mm]	[c]
97	SPR-POT 15	RC-GLT relative horizontal displacement, 2nd storey [mm]	[c]
98	SPOT 1	CLT deformation, 2nd storey [mm]	—
99	SPOT 2	CLT deformation, 1st storey [mm]	—
100	SPOT 3	CLT deformation, 2nd storey [mm]	[a]
101	SPOT 4	Internal infill deformation, 2nd storey [mm]	—
102	SPOT 5	CLT deformation, 2nd storey [mm]	n/a
103	SPOT 8	CLT deformation, 2nd storey [mm]	n/a
104	SPOT 9	CLT deformation, 2nd storey [mm]	[a]
105	SPOT 12	Internal infill deformation, 1st storey [mm]	—
106	SPOT 13	CLT deformation, 2nd storey [mm]	—
107	SPOT 14	Internal infill deformation, 1st storey [mm]	—
108	SPOT 15	Internal infill deformation, 2nd storey [mm]	[a]
109	C1	Column C1 axial force [kN]	—
110	C2	Column C2 axial force [kN]	—
111	C3	Column C3 axial force [kN]	—

[a]Data not usable due to instrument malfunction in test 6: "Retrofitted specimen Stage2."
[b]Instrument readings exhibit drift, attributed to friction at the tip or movement of its support in test 6: "Retrofitted specimen_Stage2."
[c]Instrument readings exhibit drift, attributed to tip friction or movement in test 5: "Retrofitted specimen Stage1."
[d]Instrument reached upper/lower measurement limit; data saturated at maximum range in test 5: "Retrofitted specimen Stage2."
[e]Instrument reached upper/lower measurement limit; data saturated at maximum range.

2.2 | Test Setup

The specimens were constructed on a reinforced concrete foundation beam rigidly anchored to the strong floor of the STRULAB laboratory at the University of Patras. Vertical loads were applied to the three columns through a system of two pre-tensioned steel threaded bars per column, reacting against the strong floor. Each bar was equipped with a disc-spring assembly, which helped maintain the applied load (200 kN per column) approximately constant by compensating for frame displacements and limiting load unbalance between columns, and a load cell to continuously monitor the applied forces.

Lateral loading was applied at the central beam–column joints of each storey (Figure 3). For this purpose, special reinforced concrete stubs were cast as elements (corbels) protruding the frame width, with the same depth as the beams (40 cm) and increased width (35 cm) to guarantee shear capacity under actuator loads. To avoid weak interfaces, the stubs were cast with a high-strength concrete, and post-tensioned at 300 kN per storey using high-strength strands to enhance their stiffness. Four servo-controlled actuators (two per storey) were connected to these stubs and operated in a coordinated manner to reproduce an inverted triangular force distribution: at the top storey, one actuator was displacement-controlled and the other slaved (in displacement terms) to it; at the lower storey, one actuator was force-controlled (half the top force) and the other slaved to its displacement.

In addition to the cyclic protocol, snap-back tests were carried out prior to the main loading sequence by imposing a small initial displacement at the top of the frame and then suddenly releasing it. The release was enabled by a fuse-like element (Figure 4) with known mechanical properties which connected the specimens to the reaction wall. The instantaneous stress release of the fuse-like element triggered free vibrations of the specimens, which made it possible to investigate their dynamic behavior. The resulting free vibration of the structures (in the as-built and retrofitted configurations) was recorded through the dedicated instrumentation, as illustrated in Figure 4. A comprehensive series of material characterization tests was performed comprising testing of concrete cubes in compression, tensile testing of steel rebars used as reinforcement for the specimens, flexural testing of mortar prisms, compression testing of mortar "cubes" obtained from the bending specimens, testing of bricks and blocks in compression, testing of masonry prisms in compression, shear testing of masonry prisms, tension testing (pull-out tests) of the screw fasteners from the RC frame (performed after the main testing campaign), and shear testing (pushout tests) of the screw fasteners installed to the concrete surface. Elaborated numerical results obtained from the above tests are provided in Giongo, Graziotti, Stathas, et al. (2025).

2.3 | Instrumentation

The instrumentation layout was designed to capture both the global response of the frames and the local behavior of the infills and retrofitting components. As already mentioned in Section 2.2, the vertical load systems were monitored through load cells installed on each threaded bar, ensuring continuous control of the applied axial forces.

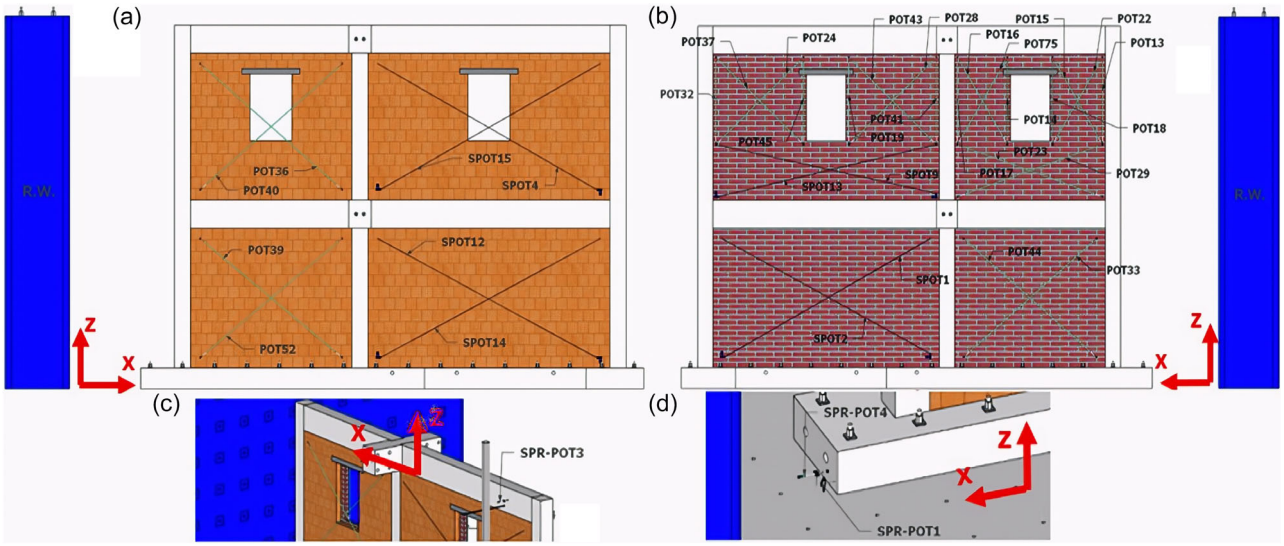

FIGURE 6 | Instrument ID for As-built specimen: (a) hollow bricks wythe, (b) solid bricks wythe, (c) out of plane response, and (d) foundation uplift and sliding.

During the snap-back tests, four accelerometers and a high-accuracy displacement transducer (Temposonic type) were installed (Figure 5). The accelerometers were placed one at each storey and oriented in both in-plane and out-of-plane directions, while the displacement transducer was used to measure the top displacement of the specimen. These instruments provided the data necessary to identify the initial dynamic properties of the frames before the onset of cyclic loading.

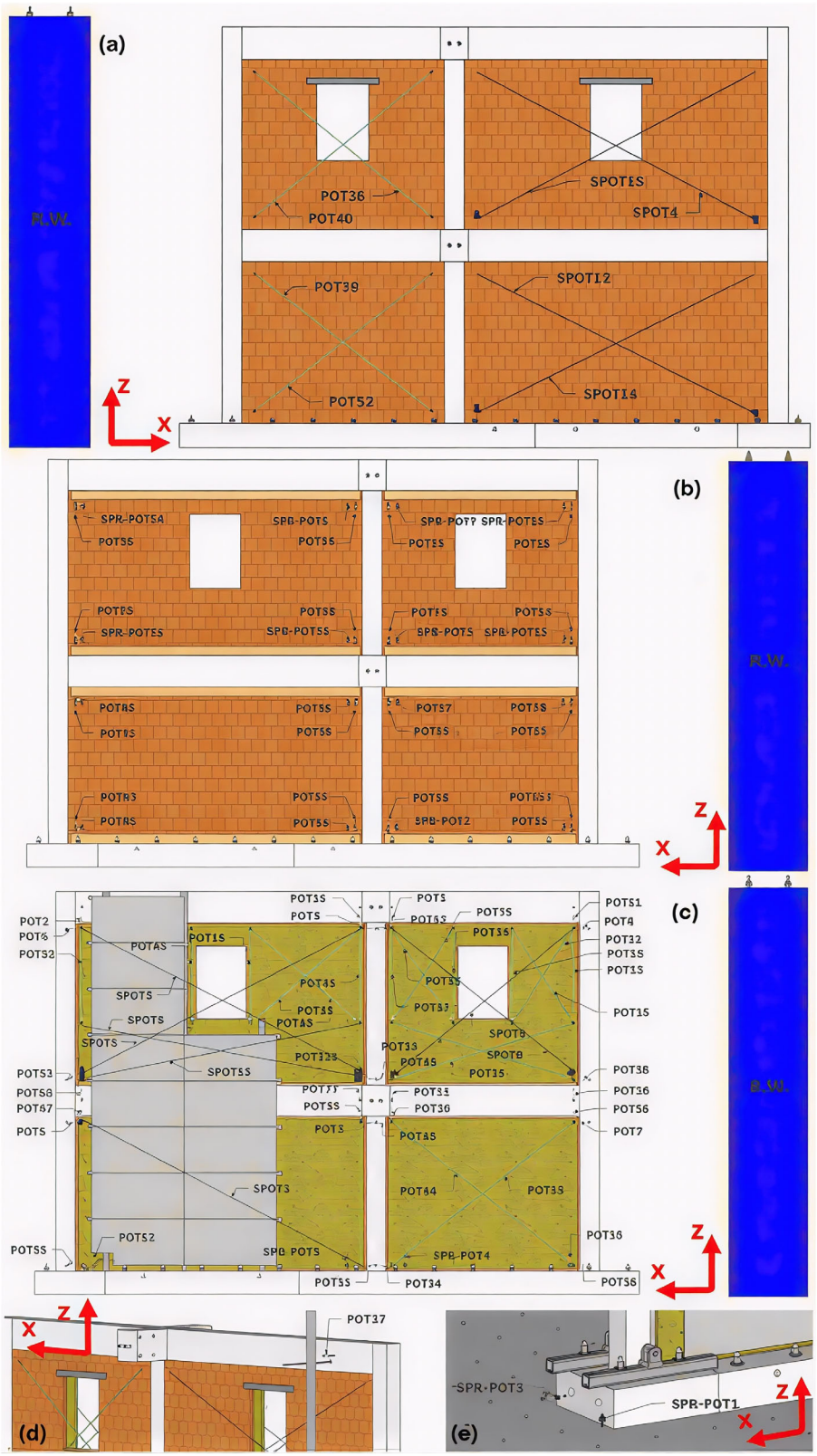

FIGURE 7 | Instrument ID for Retrofitted specimen: (a) hollow bricks wythe, (b) timber subframe response, (c) CLT panel side, (d) out of plane response, (e) foundation uplift and sliding.

For the cyclic tests, in the as-built frame potentiometers were dedicated to measure the in-plane deformation of the masonry infills, with separate sensors applied to the external wythe of solid bricks and the internal wythe of hollow blocks. In the retrofitted specimen, the instrumentation was instead arranged to characterie the behavior of the timber retrofit: one group of potentiometers measured the in-plane deformation of the CLT panels, another recorded he relative slip between the panels and the RC frame, and a third monitored the relative displacement between the glulam subframe and the RC members.

All sensors were distributed symmetrically on each bay and storey, ensuring redundancy and enabling a detailed reconstruction of both the global hysteretic response and the local interaction phenomena between RC frame, infills, and retrofit system. Their recordings were synchronized to applied loads and deformation.

3 | The Dataset

Recording of the sensors during each test was synchronous with measurements being stored in the comma-separated-value (csv) files available in Zenodo repository. Data post-processing comprised zero offsetting (except for axial load measurements) and filtering via a Savitzky–Golay filter—no other post-processing action was taken. A separate data file is provided for each test, with file naming following the designation provided in Table 3. Accelerations are expressed in [g], displacements in [mm], and forces in [kN]. Recorded signals marked as "n/a" in the last column of Tables 4, 5, and 6, refer to sensors being offline or removed for approaching their measuring capacity during testing.

Focusing on the provided data, a few sensors (indicated in the following Tables) exhibit saturation at specific intervals. This behavior is attributed to the sensors reaching their maximum measurement capacity, and it should be taken into consideration during the interpretation of the recorded data. Furthermore, some sensors signal (appropriately indicated in the following Tables) exhibit drift, which is related to the sensor tip friction or a slight deformation of the sensor's anchorage base. This effect should likewise be considered by users when evaluating the results. Finally, a number of sensors (appropriately indicated in the following Tables) malfunctioned during the testing campaign and consequently, the data obtained from these sensors are unreliable and should not be taken into consideration.

The structure of information provided, including the data stored in each column, is summarized in Table 4, 5, and 6. In these tables, the "Col." column refers to the column number in the data matrix, while "Instrument ID" corresponds to the instrument identifier shown in Figure 6 (As-built specimen) and Figure 7 (Retrofitted specimen). The "Description" column provides a brief explanation of the instrument, the "Sign convention" column specifies the adopted sign convention for the corresponding instrument, and the "Notes" column reports additional details regarding the instruments.

The sign convention for each instrument type is as follows: for the actuators, positive and negative forces denote movements towards (−x) and away from (+x) the loading frame, respectively, as illustrated in Figure 3. The same convention is adopted for all four actuators. For potentiometers and wire potentiometers a positive sign (+) signals elongation, whereas a negative sign (−) signals shortening. For the snap-back setup, the sign conventions of both the accelerometers and the high-accuracy displacement transducer (Temposonic) are consistent with the reference system shown in Figure 5.

4 | Concluding Remarks

The data study presents the metadata of an experimental program investigating at large-scale a timber-based RC–TP retrofitting technique on a two-storey, two-bay RC frame representative of mid-20th century European construction practice, and comparing it to that of an identical, as-built, frame. The dataset (openly available at Zenodo repository) comprises results from both cyclic and snap-back tests on each specimen, and the recordings of a broad spectrum of response parameters: global and local deformation parameters of masonry infills and cross-laminated timber panels, relative displacements at connections, and free-vibration properties prior to damage. Compared with past single-storey, single-bay investigations, this campaign introduces additional aspects and novelties, such as the presence of window openings, the retention of the internal masonry wythe, the adoption of dry mechanical connections between the RC frame and the glulam subframe, and the examination of the compatibility of the retrofitting measures to nonstructural finishing layers (e.g., ventilated façade systems). The metadata provided here complement the actual dataset by describing thoroughly the typology and topology of the sensors used to capture the response at both global and local level thus enabling calibration/validation of numerical models, comparative studies on retrofit strategies, and development of guidelines for integrated seismic and energy upgrading of existing RC buildings.

Acknowledgments

The work presented in the present report is part of the transnational access project "ERIES-STRONG," supported by the Engineering Research Infrastructures for European Synergies (ERIES) project (www.eries.eu), which has received funding from the European Union's Horizon Europe Framework Programme under grant agreement no. 101058684. This is ERIES publication number D8. In addition, 2024–2026 ReLUIS-DPC network (Italian University Network of Seismic Engineering Laboratories and Italian Civil Protection Agency) is acknowledged for supporting the user team in the development of analytical and numerical tools used for the specimen and retrofit design. XLAM DOLOMITI S.p.s. and PYTHON fixings Ltd. are also thanked for providing respectively the timber material and the connections (i.e., timber-to-concrete and timber-to-masonry connections) necessary for retrofitting the specimen with the RC-TP technique.

The publication of this article in OA mode was financially supported by HEAL-Link.

Funding

The work presented in the present report is part of the transnational access project "ERIES-STRONG", supported by the Engineering Research Infrastructures for European Synergies (ERIES) project (www.eries.eu), which has received funding from the European Union's Horizon Europe Framework Programme under Grant Agreement No. 101058684. This is ERIES publication number D8.

Conflicts of Interest

The authors declare no conflicts of interest.

Data Availability Statement

The dataset presented in this article is openly available for download from the Zenodo database at https://doi.org/10.5281/zenodo.17443702.

References

Bartolotti, A., F. Smiroldo, and I. Giongo. 2024. "Nonlinear Dynamic Study on Existing Masonry-Infilled Concrete Frames Retrofitted with Timber Panels." In *Structures*, Vol. 69, 107328. Elsevier. https://doi.org/10.1016/j.istruc.2024.107328.

Demirel, I. O., A. Yakut, and B. Binici. 2022. "Seismic Performance of Mid-Rise Reinforced Concrete Buildings in Izmir Bayrakli after the 2020 Samos Earthquake." *Engineering Failure Analysis* 137: 106277. https://doi.org/10.1016/j.engfailanal.2022.106277.

Giongo, I., F. Graziotti, A. Marini, and M. Valluzzi. 2025, "TIMBER-BASED RETROFIT STRATEGIES FOR EXISTING URM AND RC STRUCTURES: INSIGHT FROM RELUIS-DPC PROJECT," *Timber-Based Retrofit Strategies for Existing URM and RC Structures: Insight from ReLUIS-DPC Project." In Proceedings of the 14th World Conference on Timber Engineering: Advancing Timber for the Future Built Environment (WCTE 2025).* https://doi.org/10.52202/080513-0185.

Giongo, I., F. Graziotti, N. Stathas, et al. 2025. "Seismic Retrofitting of RC Buildings Using Cross-Laminated Timber Panels: Insights from the ERIES-STRONG Project." In *International Workshop in Engineering Research Infrastructures for European Synergies*, 255–267. https://doi.org/10.1007/978-3-031-98893-6_24.

Hassan, W. M., and J. P. Moehle. 2012. "Experimental Assessment of Seismic Vulnerability of Corner Beam-Column Joints in Older Concrete Buildings." In *Proceedings of the 15th World Conference on Earthquake Engineering, 24–28 September 2012, Lisbon, Portugal*.

Iovane, G., A. Sandoli, D. Marranzini, R. Landolfo, A. Prota, and B. Faggiano. 2023. "Timber Based Systems for the Seismic and Energetic Retrofit of Existing Structures." *Procedia Structural Integrity* 44: 1870–1876. https://doi.org/10.1016/j.prostr.2023.01.239.

Kallioras, S., D. Bournas, F. Smiroldo, I. Giongo, M. Piazza, and F. J. Molina. 2024. "Cross-Laminated Timber for Seismic Retrofitting of RC Buildings: Substructured Pseudodynamic Tests on a Full-Scale Prototype." *Earthquake Engineering & Structural Dynamics* 53, no. 14: 4354–4378. https://doi.org/10.1002/eqe.4222.

Masi, A., L. Chiauzzi, G. Santarsiero, et al. 2019. "Seismic Response of RC Buildings During the Mw 6.0 August 24, 2016 Central Italy Earthquake: The Amatrice Case Study." *Bulletin of Earthquake Engineering* 17, no. 10: 5631–5654. https://doi.org/10.1007/s10518-017-0277-5.

Meireis, C., F. S. Serino, C. Maia, A. C. Fontes, and J. M. Branco. 2022. "Current Practice and Potential Associated with Timber-Based Solutions for Buildings Retrofitting." *Infrastructures* 7, no. 2: 25. https://doi.org/10.3390/infrastructures7020025.

Pavese, A., I. Lanese, and R. Nascimbene. 2016. "Seismic Vulnerability Assessment of an Infilled Reinforced Concrete Frame Structure Designed for Gravity Loads." *Journal of Earthquake Engineering* 21, no. 2: 267–289. https://doi.org/10.1080/13632469.2016.1172372.

Pampanin, S., G. M. Calvi, and M. Moratti. 2002. "Seismic Behaviour of RC Beam-Column Joints Designed for Gravity Loads." In *Proceedings of the 12th European Conference on Earthquake Engineering, 9–13 September 2002, London, UK*.

Ricci, P., F. De Luca, and G. M. Verderame. 2011. "6th April 2009 L'Aquila Earthquake, Italy: Reinforced Concrete Building Performance." *Bulletin of Earthquake Engineering* 9, no. 1: 285–305. https://doi.org/10.1007/s10518-010-9204-8.

Sezen, H., A. S. Whittaker, K. J. Elwood, and K. M. Mosalam. 2003. "Performance of Reinforced Concrete Buildings during the August 17, Kocaeli, Turkey Earthquake, and Seismic Design and Construction Practice in Turkey." *Engineering Structures* 25, no. 1: 103–114. https://doi.org/10.1016/S0141-0296(02)00121-9.

Smiroldo, F., I. Giongo, and M. Piazza. 2021. "Use of Timber Panels to Reduce the Seismic Vulnerability of Concrete Frame Structures." *Engineering Structures* 244: 112797. https://doi.org/10.1016/j.engstruct.2021.112797.

Smiroldo, F., S. Kallioras, G. Sommacal, D. Bournas, M. Piazza, and I. Giongo. 2023. "Full-Scale Testing of Masonry-Infilled RC Frames Retrofitted with Cross-Laminated Timber Panels." *Engineering Structures* 294: 116789. https://doi.org/10.1016/j.engstruct.2023.116789.

Vuran, E., C. Serhatoğlu, M. Ö. Timurağaoğlu, E. Smyrou, İ. E. Bal, and R. Livaoğlu. 2025. "Damage Observations of RC Buildings from 2023 Kahramanmaraş Earthquake Sequence and Discussion on the Seismic Code Regulations." *Bulletin of Earthquake Engineering* 23, no. 3: 1153–1182. https://doi.org/10.1007/s10518-023-01843-3.